Article

Supramolecular Conformational Effects in the Electrocatalytic Properties of Electrostatic Assembled Films of *Meso*(3- and 4-Pyridyl) Isomers of Tetraruthenated Porphyrins

Ildemar Mayer[a], Marcos N. Eberlin[b], Daniela M. Tomazela[b], Henrique E. Toma[a] and Koiti Araki*,[a]

[a] *Instituto de Química, Universidade de São Paulo, CP 26077, 05513-970 São Paulo - SP, Brazil*

[b] *Instituto de Química, Universidade Estadual de Campinas, CP 6154, 13083-970 Campinas - SP, Brazil*

Meso (3- e 4-piridil)porfirinas coordenadas a quatro complexos [Ru(bipy)$_2$Cl]$^+$, M(3-TRPyP) e M(4-TRPyP), onde M = 2H$^+$ e Zn^{2+}, foram obtidas e caracterizadas por métodos eletroquímicos, espectroscopia e espectrometria de massas. Os filmes eletrostaticamente montados camada por camada com ftalocianina de cobre tetrassulfonada, CuTSPc, apresentaram atividade eletrocatalítica diferenciada para a oxidação de sulfito e nitrito. Em geral, os filmes derivados dos isômeros M(4-TRPyP) são mais ativos para a oxidação de nitrito, enquanto aqueles contendo os isômeros M(3-TRPyP) são mais eficientes para a oxidação de sulfito. Os resultados revelaram uma influência significativa da geometria molecular no sítio ativo dos nanomateriais porfirínicos, que favorece os processos de transferência eletrônica nos derivados de M(3-TRPyP), através de mudanças no empacotamento molecular com a CuTSPc.

Meso(3- and 4-pyridyl)porphyrins coordinated to four [Ru(bipy)$_2$Cl]$^+$ complexes, M(3-TRPyP) or M(4-TRPyP), where M=2H$^+$ and Zn^{2+}, have been obtained and characterized by electrochemistry, spectroscopy and mass spectrometry. Layer-by-layer electrostatic assembled films with tetrasulfonated phthalocyaninatecuprate(II) anion, CuTSPc, displayed distinct electrocatalytic activity towards sulfite and nitrite oxidation. In general, the films derived from the M(4-TRPyP) isomers are more effective for the oxidation of nitrite, whereas those containing the M(3-TRPyP) isomers are more efficient for the oxidation of sulfite. The results demonstrated the influence of molecular geometry on the active sites of porphyrinic nanomaterials, enhancing the electron-transfer process in the M(3-TRPyP) derivative. This effect results from changes in the chemical environment around the active sites, induced by the contrasting molecular packing interactions with CuTSPc.

Keywords: supramolecular chemistry, metalloporphyrins, electrostatic assembled films, electrocatalysis, electrochemistry, mass spectrometry

Introduction

Metalloporphyrins have been of great interest in the design of supramolecular systems because their electrochemical, photochemical and catalytic properties can be modulated by employing suitable ancillary bridging transition-metal complexes.[1-7] In such systems, the ancillary complexes can either modify the local environment around the porphyrin ring, improving the solvation and solubility properties, or act as cofactors in redox processes providing electron acceptor-donor sites and relays. They can also modify the intrinsic activity of the metalloporphyrin center by means of electronic interactions, and contribute with additional sites for intra-

and intermolecular interactions, allowing the assembly of higher order supramolecular structures and materials.

The electrocatalytic properties of porphyrins in homogeneous and heterogeneous systems[7-20] have attracted considerable attention, particularly for multielectronic processes such as the 4-electron reduction of dioxygen to water;[21,22] and the reduction of dinitrogen[11,16,23] and sulfur compounds.[24,25] Such investigations can be conveniently performed by immobilizing molecular materials on a solid electrode surface.[26] They should be deposited preferentially as thin adherent, stable and electrochemically active films generated by dip-coating, electrostatic assembly or electropolymerization methods.[27-29]

The electrocatalytic properties of cobalt and nickel tetra(4-pyridyl)porphyrins bound to four [Ru(bipy)$_2$Cl]$^+$ complexes, *i.e.*, M(4-TRPyP), have already been investigated

* e-mail: koiaraki@iq.usp.br

in our laboratory.[7] The coordination of the ruthenium complexes provide a very rich electrochemistry, enhancing the electrocatalytic properties for the oxidation of nitrite, sulfite, ascorbic acid, phenol and dopamine.[17,30-36] Similar studies focusing on the tetra(3-pyridyl)porphyrin analogues, M(3-TRPyP), have never been reported. These novel supramolecular species are especially interesting because the ancillary complexes tend to adopt, for steric reasons, an out of plane configuration with respect to the porphyrin ring (Figure 1). The influence of such structural effect on the spectroscopic and electrochemical properties has been discussed with the support of molecular modeling calculations.[37] Such differences in stereochemistry are expected to change the electrocatalytic properties of such materials, for example improving the activity or selectivity. For this reason and as reported herein, new M(3-TRPyP) complexes have been synthesized and an extensive characterization of their structure and properties has been performed based on ESI-MS, tandem ESI-MS/MS, UV-Vis spectroscopy and spectroelectrochemistry.

Although molecular films of M(4-TRPyP) and M(3-TRPyP) can be generated by dip-coating or drop-casting from a methanol solution, their solubility in water is high enough to preclude their use. To render such films virtually insoluble in aqueous solutions,[29,38] a layer-by-layer electrostatic assembly with a suitable negatively charged species, more specifically the tetrasulfonated phthalocyaninatecuprate(II) anion (CuTSPc), has been performed. The electrocatalytic properties of the films assembled from both isomers were investigated on a comparative basis, in order to evaluate the supramolecular conformational effects on the oxidation of nitrite and sulfite in aqueous solution.

Experimental

The solvents and reagents were of analytical grade and used without further purification, unless otherwise stated. M(4-TRPyP) was previously obtained and M(3-TRPyP) were prepared by metathesis of M(3-TPyP) and [Ru(bipy)$_2$Cl$_2$] (1:4.1 molar ratio) in glacial acetic acid, following the same procedure.[39]

The cyclic voltammograms were obtained in DMF and CH$_3$CN or in an aqueous solution using an AUTOLAB PGSTAT30 potentiostat/galvanostat from Ecochemie. A conventional three electrodes cell, consisting of a platinum disk working electrode, Ag↳Ag$^+$ (0.010 mol dm^{-3} in CH$_3$CN) reference electrode and a coiled platinum wire auxiliary electrode was employed. The same arrangement, except for the Ag↳AgCl↳KCl 1.00 mol dm^{-3} reference electrode, was used in the electrochemical studies of M(TRPyP)/CuTSPc
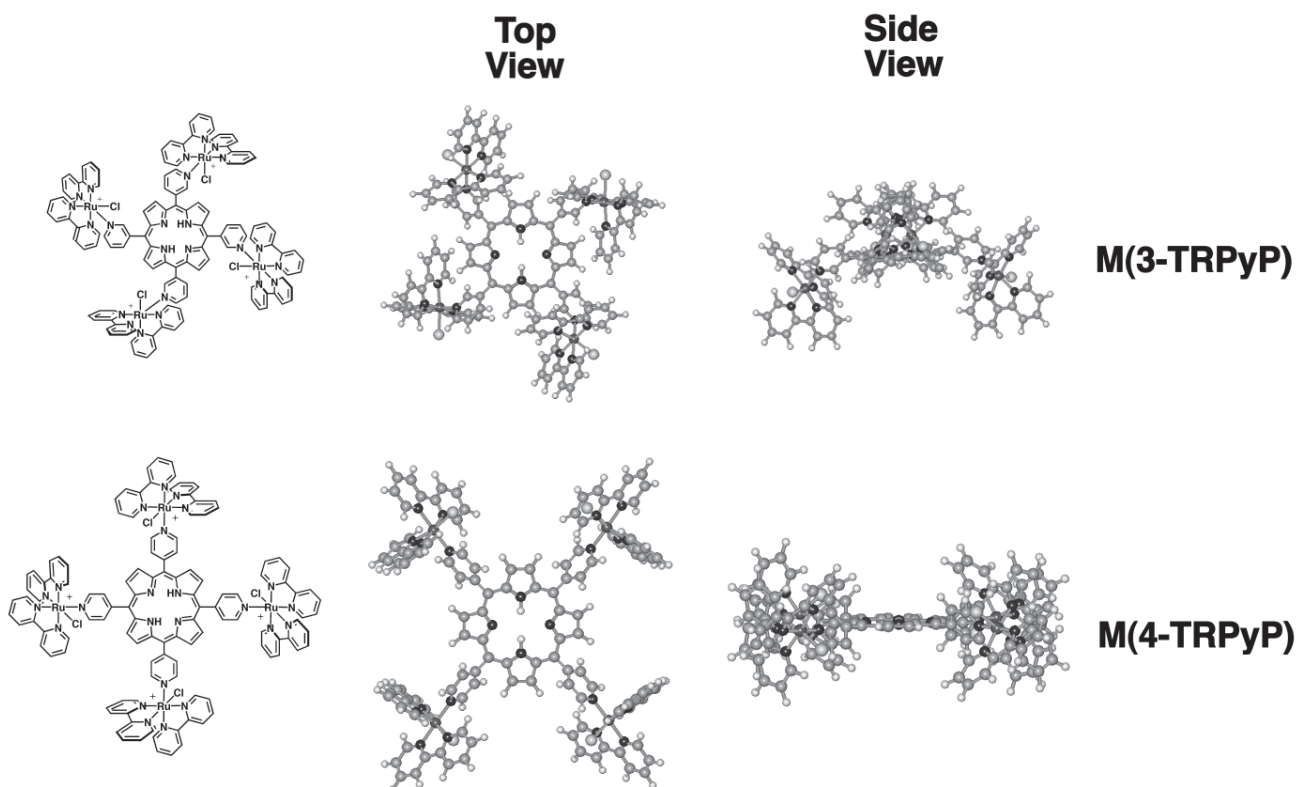
Figure 1. Structures of the M(3-TRPyP) and M(4-TRPyP) isomers, where M is 2H$^+$ or Zn^{2+}. Top and side views of the geometry optimized structures by modified MM2(91) force field calculations, employing the HyperChem^{TM} program.

film modified glassy carbon electrodes. All potentials were converted to the SHE scale by adding 0.503 or 0.222 V to the experimental values in organic or in aqueous solution, respectively. A phosphate buffered (pH 6.80) 0.50 mol dm^{-3} KNO_3 solution was utilized as aqueous electrolyte. The spectroelectrochemistry data were collected using a thin-layer cell and an EG&G 173 potentiostat/galvanostat and a HP8453 diode-array spectrophotometer.

Electrospray mass spectra were recorded on a Q-Tof (Micromass) mass spectrometer with a quadrupole (Qq) and high-resolution orthogonal time of flight (o-TOF) configuration. Samples dissolved in pure methanol were injected through an uncoated fused-silica capillary, using a syringe pump (Harvard Apparatus, Pump 11, 10μdm^{-3} min^{-1}). The ESI-MS mass spectra were acquired using an ESI capillary voltage of 3 kV and a cone voltage of 10 V. Isotopic patterns were calculated using the MassLynx software.

Results and Discussion

Mass Spectrometry

The tetraruthenated porphyrin species were thoroughly characterized by mass spectrometry, each complex showing characteristic ESI mass spectrum. Collision-induced dissociation of their cationic species as observed in their ESI tandem mass spectra follows, however a common mechanism, *i.e.*, the stepwise rupture of the Ru–N(pyP) bonds leading successively to less and less positively charged species and finally to the corresponding neutral M(TPyP) species.[40] Accordingly, the mass spectrometry characterization will be detailed only for the Zn(3-TRPyP) which exhibited the $[C_{120}H_{88}N_{24}ZnRu_4Cl_4]^{4+}$ (MM = 2477.65 g mol^{-1}) a complex isotope cluster with a principal ion of *m/z* 619 and Δ(*m/z*) 0.25 as expected for a tetracationic species with various multi-isotope elements. This ion loses one to three $[Ru(bipy)_2Cl]^+$ cationic fragments of *m/z* 449 and Δ(*m/z*) 1, leading respectively to $[C_{100}H_{72}N_{20}ZnRu_3Cl_3]^{3+}$ of *m/z* 676, Δ(*m/z*) = 0.33, $[C_{80}H_{56}N_{16}ZnRu_2Cl_2]^{2+}$ of *m/z* 790, Δ(*m/z*) 0.50, and $[C_{60}H_{40}N_{12}ZnRuCl]^+$ of *m/z* 1130, Δ(*m/z*) =

1. The relatively light and quadruply-charged gaseous ion is considerably stable because the positive charges are not localized, but rather spread on the peripheral groups. However, its high charge state as well as that of the triply–charged ion leads to quite strong electrostatic interactions with anions, as confirmed by its tendency to be transferred to the gas phase as ion-paired species. Accordingly, the ions of *m/z* 876 (Δ(*m/z*) 0.33) and 1088 (Δ(*m/z*) 0.50), are assigned to $[C_{120}H_{88}N_{24}ZnRu_4Cl_4(CF_3SO_3^-)]^{3+}$ and $[C_{100}H_{72}N_{20}ZnRu_3Cl_3(CF_3SO_3^-)]^{2+}$ species. Another possibility is the coordination of Lewis bases such as the solvent methanol to a Zn(II) axial position,[41] as attested by the ions of *m/z* 627 (Δ(*m/z*) 0.25) and 687 (Δ(*m/z*) 0.33) attributed to $[C_{120}H_{88}N_{24}ZnRu_4Cl_4(CH_3OH)]^{4+}$ and $[C_{100}H_{72}N_{20}ZnRu_3Cl_3(CH_3OH)]^{3+}$, respectively. All assignments were confirmed by the corresponding ESI-MS/MS spectra, using the collision induced dissociation (CID) technique. Scheme 1 summarizes the dissociation routes of [Zn(3-TRPyP)]$^{4+}$ whereas Table 1 summarizes the ESI mass spectrum in the positive ion mode of the [Zn(3-TRPyP)](CF$_3$SO$_3^-$)$_4$ complex with ion assignments.

Spectroelectrochemistry

Both free-base derivatives, H$_2$(3-TRPyP) and H$_2$(4-TRPyP), exhibit characteristic spectroscopic and electrochemical properties,[7,40,42] associated with the porphyrin and ruthenium polypyridine moieties. The coordination of a transition metal ion such as Zn(II) to the porphyrin ring leads to a decrease in the solubility and a shift of the Soret band from 415 to 428 nm. Also, the four visible bands at 515, 548, 590 and 645 nm of the free-base species changed to a two bands pattern at 561 and 599 nm, respectively, in ethanol.

The coordination of Zn(II) to the porphyrin ring has a significant influence on the electronic and electrocatalytic properties, as shown below. The absorption spectrum of the Zn(II) derivative[43] is very susceptible to the bonding of an axial ligand. For example, the stepwise addition of 20 μdm^3 of H$_2$O in a Zn(3-TRPyP) acetonitrile solution, leads to an

Table 1. Assignments for the cations observed in the ESI(+) mass spectrum of [Zn(3-TRPyP)](CF$_3$SO$_3^-$)$_4$ complex

| Assignment	MM (g mol^{-1})	*m/z* exp. (calc.)	Relative Intensity
$[C_{120}H_{88}N_{24}ZnRu_4Cl_4]^{4+}$	2477.6	619.6 (619.4)	81
$[C_{100}H_{72}N_{20}ZnRu_3Cl_3]^{3+}$	2028.6	676.4 (676.2)	100
$[C_{80}H_{56}N_{16}ZnRu_2Cl_2]^{2+}$	1579.6	789.5 (789.8)	20
$[C_{60}H_{40}N_{12}ZnRuCl]^+$	1130.6	1130.5 (1130.6)	02
$[Ru(bipy)_2Cl]^+$	449.0	449.1 (449.0)	CID
$[C_{120}H_{88}N_{24}ZnRu_4Cl_4(CF_3SO_3^-)]^{3+}$	2626.7	876.1 (875.6)	85
$[C_{100}H_{72}N_{20}ZnRu_3Cl_3(CF_3SO_3^-)]^{2+}$	2177.6	1088.2 (1088.8)	25
$[C_{120}H_{88}N_{24}ZnRu_4Cl_4(CH_3OH)]^{4+}$	2509.6	627.5 (627.4)	14
$[C_{100}H_{72}N_{20}ZnRu_3Cl_3(CH_3OH)]^{3+}$	2060.6	686.6 (686.9)	02
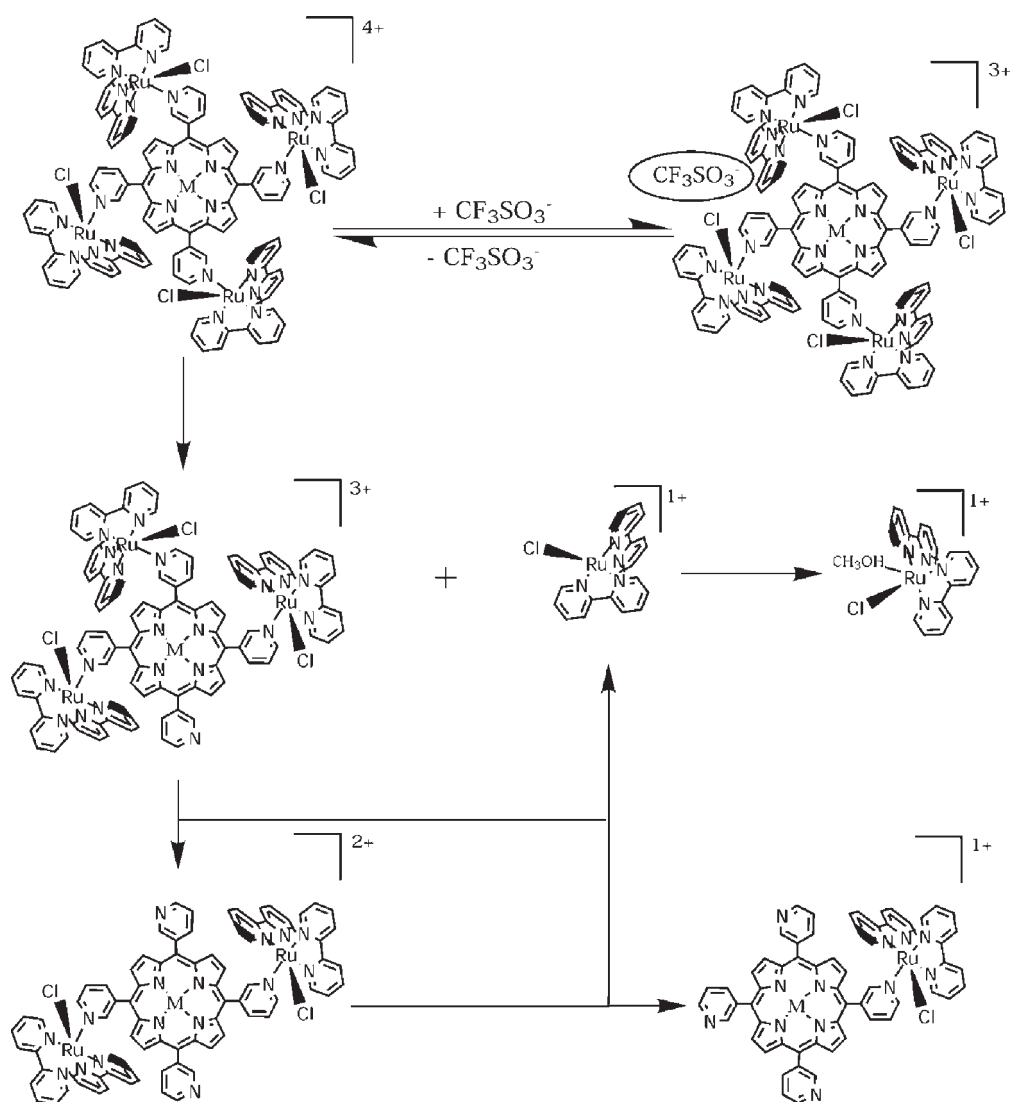
Scheme 1. Collision-induced dissociation routes of $[M(3\text{-}TRPyP)]^{+4}$, which is analogous to those observed for the corresponding $[M(4\text{-}TRPyP)]^{+4}$ isomers.

hipsochromic shift of the Soret band from 438 to 428 nm, and the shift of the Q bands from 571 and 613 to 560 and 599 nm, respectively, with well-defined isosbestic points at 396, 433, 565 and 602 nm. Such evidences indicate a simple equilibrium involving the exchange of axially coordinated CH_3CN by H_2O, and a constant $K = 7.4 \times 10^{-1} \, mol^{-1} \, dm^3$ was determined. However, a batochromic shift of the zinc porphyrin bands to 434, 570 and 610 nm was observed instead and a higher equilibrium constant $K = 1.3 \times 10^3 \, mol^{-1} \, dm^3$ was found, when water was substituted by imidazol. The behavior described above is characteristic of zinc porphyrins, where the LUMO is preferentially stabilized by ligands with π-backbonding capability,[41,43,44] decreasing the energy of the π-π^* transitions.

The cyclic voltammograms of the Zn(II) complex in DMF are shown in Figure 2 and compared with the corresponding M(4-TRPyP) in Table 3. The reversible pair of waves at 0.92 V assigned to the Ru(III/II) process is not sensitive to the coordination of Zn(II) ion, but the $H_2(3\text{-}TRPyP)$ species showed that process at 0.88 V (Figure 2A). The anodic peaks found around 1.3 to 1.6 V, with a typical EC mechanism behavior, were assigned to the oxidation of the porphyrin ring to the radical cation or dication.[7,40,42]

Going to the negative side, one or two pairs of waves were found in the –0.5 to –1.2 V range. The reduction of the porphyrin ring occurs in two stepwise monoelectronic processes, leading to the radical anion and dianion respectively (Table 3). The free-base complex exhibited the first reduction process at –0.68 V and the Zn(II) derivative at –0.97 V, while the second reduction potentials showed-up around –1.0 and –1.17 V respectively. The subsequent reduction processes are localized on the
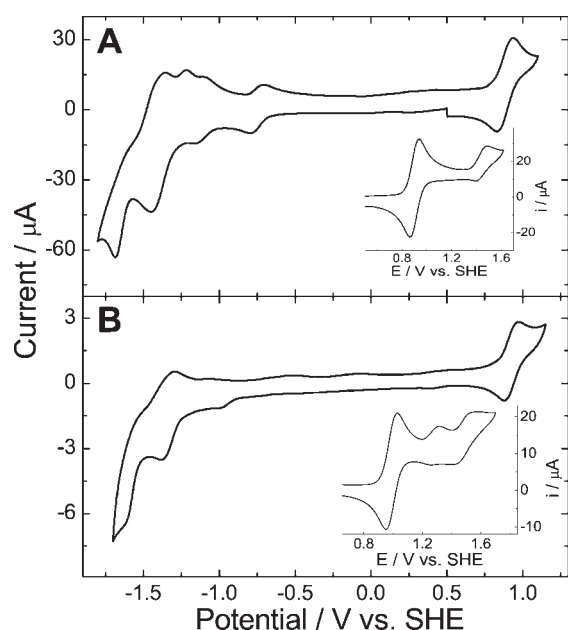
Figure 2. Cyclic voltamograms of the (A) H$_2$(3-TRPyP) v = 100 mV s^{-1} and (B) Zn(3-TRPyP) v = 20 mV s^{-1}, in DMF solution containing 0.10 mol dm^{-3} of TEAClO$_4$, in a Pt electrode. **Inset:** CVs of (A) H$_2$(3-TRPyP) and (B) Zn(3-TRPyP) extended to more positive potentials.

peripheral ruthenium bipyridine complexes, more specifically on the bipyridine ligands, and should reflect the electronic effects induced by the metalloporphyrin. Those processes were found more or less at the same potential for the M(3-TRPyP) (–1.38 and –1.63 V) and M(4-TRPyP) isomers (–1.39 and –1.67 V), but the deviation was more pronounced in the last case, probably because of the stronger electronic coupling[7,39,45,46] between the porphyrin and the ruthenium complexes.

The electrochemical processes were assigned in accordance with the spectroelectrochemistry data, which exhibited the typical behavior of the Zn(3-TRPyP) complex, shown in Figure 3. The disappearance of the Ru^{II}($d\pi$)→bipy($p\pi$*) charge-transfer band at 485 and the ligand field band at 370 nm, and the shift of the $p\pi$→$p\pi$* band of the bipy ligands from 297 to 317 nm were observed, while the porphyrin bands remained more or less unchanged, in the 0.50 to 1.20 V range (Figure 3A), as expected for the Ru(II)→Ru(III) oxidation process. The small enhancement

of the Soret band during this reaction may be indicative of the electronic coupling between the porphyrin and ruthenium complexes. The intensity of the porphyrin bands (Soret and Q) decreased very rapidly when the potential was stepped to +1.50 V and +2.00 V (Figure 3B and 3C, respectively), while the peripheral complexes bands remained almost unchanged, indicating redox processes (mono and bielectronic) involving the porphyrin ring.

Going to the negative side, the application of –1.10 V (Figure 3D) leads to the reversible shift of the Soret and Q bands from 429 to 444 nm and 560 and 599 nm to 579 and 621 nm, respectively. The presence of isosbestic points indicates that the equilibrium involves only two species, the neutral porphyrin and the radical anion. At –1.20 V (Figure 3F), the band at 444 nm disappeared and a weaker band rose at 480 nm, concomitantly with the shift of the Q bands to 602 and 636 nm, respectively, and the rise of a new broad band at 750 nm, evidencing the formation of the porphyrin dianion. The decrease of the bipyridine
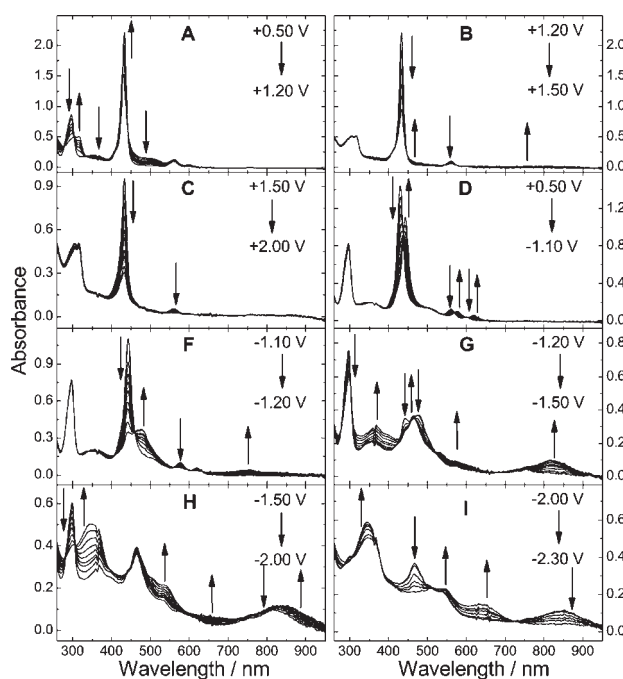
Figure 3. Spectroelectrochemistry of Zn(3-TRPyP)] in 0.10 mol dm^{-3} TEAClO$_4$ DMF solution, in the 1.50 to –2.30 V range.

Table 2. Redox potentials (V *vs.* SHE) of M(TRPyP) in DMF solution. The potential of reversible processes were collected as the average of E$_{pc}$ and E$_{pa}$, while for the reduction of the bipy ligands and oxidation of the porphyrin ring (in CH$_3$CN), their corresponding peak potentials, E$_{pc}$ and E$_{pa}$, were listed

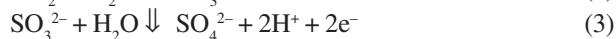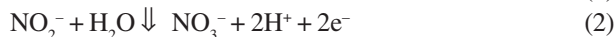| Compound	Bipy$^{-2/-1}$	Bipy$^{-1/0}$	Porph$^{-2/-1}$	Porph$^{-1/0}$	Ru$^{3+/2+}$	Porph$^{0/+1}$	Porph$^{+1/+2}$
H$_2$(3-TRPyP)	–1.63	–1.39	–1.06	–0.67	0.88	1.57	1.57
H$_2$(4-TRPyP)	–1.52	–1.42	–0.93	–0.68	0.92	1.65	1.65
Zn(3-TRPyP)	–1.62	–1.38	–1.17	–0.97	0.92	1.31	1.55
Zn(4-TRPyP)	–1.67	–1.39	–1.18	–0.97	0.92	1.31	1.31

$p\pi \rightarrow p\pi^*$ band at 297 nm is observed at potentials more negative than -1.50 V (Figure 3G), in two steps: it decreases to about half when the potential is stepped to -1.50 V, and disappears completely at more negative potentials, evidencing the stepwise reduction of the two bipy ligands to the radical anion (Figure 3H). Finally, when -2.30 V was applied (Figure 3I), a third reduction involving a bipyridine ligand was registered, leading to the disapperance of the bands at 455 and 850 nm and the rise of new bands at 640 nm. The free-base derivative showed a similar spectroelectrochemistry pattern.

Molecular films

In spite of the similarity between the spectroscopic and electrochemical properties of the M(TRPyP), it is expected that subtle differences in the electronic coupling and structural properties can be responsible for significant changes in the properties of the corresponding molecular materials. Accordingly, a thorough analysis of the electrocatalytic properties of the porphyrin films obtained by layer-by-layer electrostatic assembly both isomers with the tetra-anionic CuTSPc was carried out. The typical CVs of modified glassy carbon electrodes in aqueous solution exhibit a pair of reversible waves at 0.94 V involving the Ru(III/II) redox process, whose current increases linearly as a function of the scan rate.

The cyclic voltammograms of the modified electrodes as a function of the concentration of nitrite and sulfite, at pH 6.8, are shown in Figures 4 and 5, respectively. Note that the onset of the electrocatalytic wave for the oxidation of nitrite to nitrate (equations 1 and 2) occurred at 0.9 V and reached a maximum around 1 V, showing a relatively fast charge-transfer process mediated by a reversible redox

reaction. In addition to the current enhancement, a very significant cathodic shift of the oxidation process is apparent.

$$2Ru^{II} \Downarrow \; 2Ru^{III} + 2e^- \tag{1}$$
$$NO_2^- + H_2O \Downarrow \; NO_3^- + 2H^+ + 2e^- \tag{2}$$
$$SO_3^{2-} + H_2O \Downarrow \; SO_4^{2-} + 2H^+ + 2e^- \tag{3}$$

More interesting results were obtained when sulfite was used as substrate. Note that the oxidation to sulfate (equations 1 and 3), which is typically slow at a bare glassy carbon electrode leading to an steady increase of the current above about 0.9 V, was greatly anticipated and a very significant Faradaic current can be observed near the onset of the Ru(II/III) wave. In fact, the peak corresponding to the electrocatalytic process was found at 0.85 V (compare with $E_{1/2} = 0.92$ V), as shown in Figure 5. Furthermore, the M(3-TRPyP) isomers seems to be more efficient than the M(4-TRPyP) derivatives for that process.

In order to verify that qualitative observation in a more quantitative basis, the efficiency of the electrocatalytic processes was evaluated by plotting the catalytic current as a function of the substrate concentration. A linear correlation was obtained for the oxidation of both substrates (inset of Figure 4 and 5), in the 20 to 2000 μmol dm^{-3} range. The relative activity (electron-transfer efficiency) of the M(TRPyP)/CuTSPc layer-by-layer electrostatic assembled films can be evaluated from the angular coefficients of the current *vs.* concentration plots. These data are listed in Table 3, where it is possible to infer that the M(4-TRPyP) isomers generally are better for the oxidation of nitrite while the M(3-TRPyP) isomers are more efficient for the oxidation of sulfite. This should be reflecting the electronic and structural differences of the supramolecular tetraruthenated porphyrin
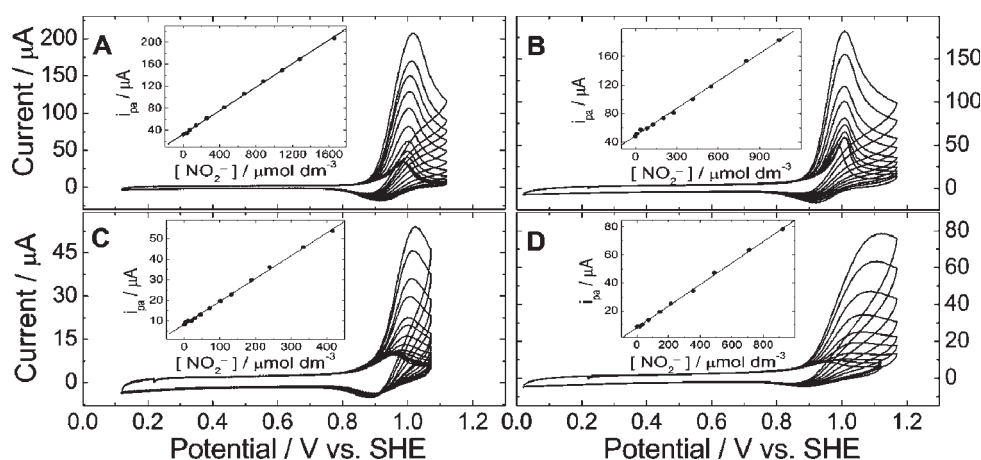
Figure 4. CVs of GC electrodes modified with layer-by-layer electrostatic assembled films of (A) H$_2$(3-TRPyP)/CuTSPc, B = 0.95 nmol cm^{-2}; (B) H$_2$(4-TRPyP)/CuTSPc, B = 0.83 nmol cm^{-2}; (C) Zn(3-TRPyP)/CuTSPc, B = 0.63 nmol cm^{-2}; (D) Zn(4-TRPyP)/CuTSPc, B = 0.79 nmol cm^{-2}; in the presence of increasing concentration of NaNO$_2$ (0.05 to 4 mmol dm^{-3} range), in pH 6.8 phosphate buffer. **Inset:** Plot of i_{pa} *vs.* [NO$_2^-$].
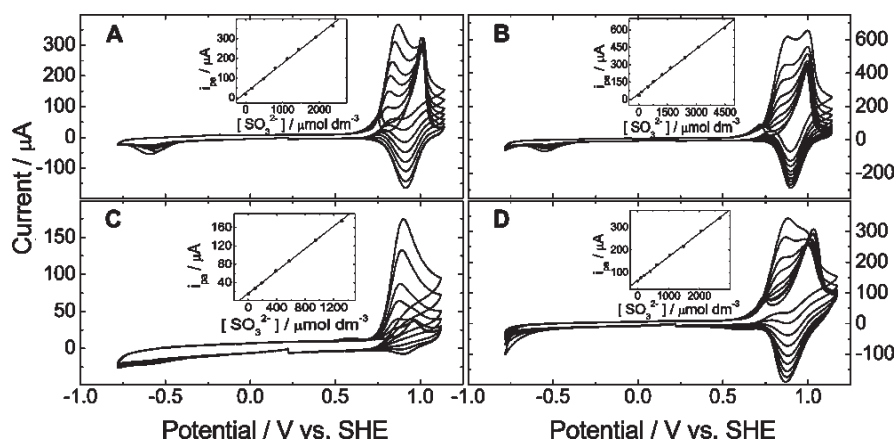
Figure 5. CVs of GC electrodes modified with layer-by-layer electrostatic assembled films of (A) H_2(3-TRPyP)/CuTSPc, B = 2.75 nmol cm^{-2}; (B) H_2(4-TRPyP)/CuTSPc, B = 3.92 nmol cm^{-2}; (C) Zn(3-TRPyP)/CuTSPc, B = 0.66 nmol cm^{-2}; (D) Zn(4-TRPyP)/CuTSPc, B = 3.32 nmol cm^{-2}; in the presence of increasing concentration of Na_2SO_3 (0.05 to 5 mmol dm^{-3} range), in pH 6.8 phosphate buffer. **Inset**: Plot of i_{pa} *vs.* [SO_3^{2-}].

species in the electrostatic assembled films. In fact, molecular modeling calculations[37] showed that the lowest energy structure of the *meta* and *para*-isomers are very different, as shown in Scheme 1. In the first one, the peripheral complexes are localized above and below the porphyrin ring and generate small pockets surrounded by [Ru(bipy)$_2$Cl]$^+$ sites, into which the sulfite ion may enter before the oxidation can take place. Notice that the CuTSPc has complementary geometry and charge. However, the potentials found for the Ru(III/II) process are all equivalent (except for the H_2(3-TRPyP) species) and the direct coordination of those substrates to the metal ion is precluded, because the ligand exchange rate is very slow. Consequently, it is surprising to see those differences in the electrocatalytic activity of the films obtained with the supramolecular porphyrin isomers, and the opposite tendencies observed for the oxidation of nitrite and sulfite may be reflecting a supramolecular conformational effect on the electron-transfer process.

Table 3. Slopes of $i_{cat.}$ *vs.* [substrate] plots. The electrocatalytic current was measured at 0.90 or 1.0 V (anodic peaks) for sulfite or nitrite oxidation, respectively

Substrate	NO$_2^-$	SO$_3^{2-}$
H_2(4-TRPyP)	128	129
H_2(3-TRPyP)	107	147
Zn(4-TRPyP)	160	105
Zn(3-TRPyP)	111	122

Conclusion

Meso-pyridylporphyrins coordinated to four [Ru(bipy)$_2$Cl]$^+$ complexes form electrocatalytic active and stable nanomaterials by layer-by-layer electrostatic assembly with tetrasulfonated phthalocyaninatecuprate(II)

anion. Interestingly, the M(3-TRPyP) and M(4-TRPyP) isomers form films with distinct activity towards oxidation of sulfite and nitrite. The M(4-TRPyP) isomers were more effective for the oxidation of nitrite while the M(3-TRPyP) isomers were more effective for the oxidation of sulfite. The differences can not be assigned to the Ru(III/II) redox potentials but rather to supramolecular conformational effects, which induced changes in the active site environment. Research are on the way to extend this study, envisaging the simultaneous analysis of more complex mixtures of analytes by exploring their specific and non-specific interactions with the porphyrin materials.

Acknowledgements

References

1. Baldini, L.; Hunter, C. A.; *Adv. Inorg. Chem.* **2002**, *53*, 213.

2. Imamura, T.; Fukushima, K.; *Coord. Chem. Rev.* **2000**, *198*, 133.

3. Wojaczynski, J.; Latos-Grazynski, L.; *Coord. Chem. Rev.* **2000**, *204*, 113.

4. Linke, M.; Chambron, S. C.; Heitz, V.; Sauvage, S. P.; Encinas, S.; Barigelletti, F.; Flamigni, L.; *J. Am. Chem. Soc.* **2000**, *122*, 11834.

5. Prodi, A.; Indelli, M. T.; Kleverlaan, C. J.; Alessio, E.; Scandola, F.; *Coord. Chem. Rev.* **2002**, *229*, 51.

6. Nakash, M.; Clyde-Watson, Z.; Feeder, N.; Teat, S. J.; Sanders, J. K. M.; *Chem. Eur. J.* **2000**, *6*, 2112.

7. Toma, H. E.; Araki, K.; *Coord. Chem. Rev.* **2000**, *196*, 307.

8. Kadish, K. M.; Smith, K. M.; Guilard, R.; *The Porphyrin Handbook,* Academic Press: Amsterdam, 2003, vols. 7, 8, 11.

9. Murakami, Y.; Kikuchi, J.; Hisaeda, Y.; Hayashida, O.; *Chem. Rev.* **1996**, *96*, 721.

10. Meunier, B.; *Chem. Rev.* **1992**, *92*, 1411.

11. Barley, M. H.; Takeuchi, K. J.; Meyer, T. J.; *J. Am. Chem. Soc.* **1986**, *108*, 5876.

12. Cheng, S. H.; Su, Y. O.; *Inorg. Chem.* **1994**, *33*, 5847.

13. Hayon, J.; Raveh, A.; Bettelheim, A.; *J. Electroanal. Chem.* **1993**, *359*, 209.

14. Pang, D. W.; Wang, Z. L.; *J. Electroanal. Chem.* **1993**, *358*, 235.

15. Chen, S. M.; Chen, S. V.; *Electrochim. Acta* **2003**, *48*, 4049.

16. Ruhlmann, L.; Genet, G.; *J. Electroanal. Chem.* **2004**, *568*, 315.

17. Casero, E.; Pariente, F.; Lorenzo, E.; *Anal. Bioanal. Chem.* **2003**, *375*, 294.

18. Lei, H. P.; Trofimova, N. S.; Ikeda, O.; *Chem. Lett.* **2003**, *32*, 610.

19. Collman, J. P.; Fu, L.; *Acc. Chem Res.* **1999**, *32*, 455.

20. Meunier, B.; Visser, S. P.; Shaik, S.; *Chem. Rev.* **2004**, *104*, 3947.

21. Shi, C. N.; Anson, F. C.; *Inorg. Chem.* **1992**, *31*, 5078.

22. Anson, F. C.; Shi, C. N.; Steiger, B.; *Acc. Chem. Res.* **1997**, *30*, 437.

23. Einsle, O.; Messerschmidt, A.; Huber, R.; Kroneck, P. M. H.; Neese, F.; *J. Am. Chem. Soc.* **2002**, *124*, 11737.

24. Rea, N.; Loock, B.; Lexa, D.; *Inorg. Chim. Acta* **2001**, *312*, 53.

25. Kline, M. A.; Barley, M. H.; Meyer, T. J.; *Inorg. Chem.* **1987**, *26*, 2197.

26. Casero, E.; Losada, J.; Pariente, F.; Lorenzo, E.; *Talanta* **2003**, *61*, 61.

27. da Rocha, J. R. C.; Demets, G. J. F.; Bertotti, M.; Araki, K.; Toma, H. E.; *J. Electroanal. Chem.* **2002**, *526*, 69.

28. Azevedo, C. M. N.; Araki, K.; Angnes, L.; Toma, H. E.; *Electroanal.* **1998**, *10*, 467.

29. Araki, K.; Wagner, M. J.; Wrighton, M. S.; *Langmuir* **1996**, *12*, 5393.

30. Bedioui, F.; Villeneuve, N.; *Electroanalysis* **2003**, *15*, 5.

31. da Rocha, J. R. C.; Angnes, L.; Bertotti, M.; Araki, K.; Toma, H. E.; *Anal. Chim. Acta* **2002**, *452*, 23.

32. Araki, K.; Winnischofer, H.; Viana, H. E. B.; Toyama, M. M.; Engelmann, F. M.; Mayer, I.; Formiga, A. L. B.; Toma, H. E.; *J. Electroanal. Chem.* **2004**, *562*, 145.

33. Wu, F. H.; Zhao, G. C.; Wei, X. W.; *Electrochem. Comm.* **2002**, *4*, 690.

34. Rocha, J. R. C.; Angnes, L.; Bertotti, M.; Araki, K.; Toma, H. E.; *Anal. Chim. Acta* **2002**, *452*, 23.

35. Azevedo, C. M. N.; Araki, K.; Toma, H. E.; Angnes, L.; *Anal. Chim. Acta* **1999**, *387*, 175.

36. Li, X.; Fu, Y.; Sun, C.; *Electroanalysis* **2003**, *15*, 1707.

37. Mayer, I.; Formiga, A. L. B.; Engelmann, F. M.; Winnischofer, H.; Oliveira, P. V.; Tomazela, D. M.; Eberlin, M. N.; Toma, H. E.; Araki, K.; *Inorg. Chim. Acta* **2005**, *in press*.

38. Toyama, M. M.; Demets, G. J. F.; Araki, K.; Toma, H. E.; *Electrochem. Comm.* **2000**, *2*, 749.

39. Engelmann, F. M.; Losco, P.; Winnischofer, H.; Araki, K.; Toma, H. E.; *J. Porphyr. Phthalocyanines* **2002**, *6*, 33.

40. Tomazela, D. M.; Gozzo, F. C.; Mayer, I.; Engelmann, F. M.; Araki, K.; Toma, H. E.; Eberlin, M. N.; *J. Mass. Spectrom.* **2004**, *39*, 1161.

41. Dovidauskas, S.; Araki, K.; Toma, H. E.; *J. Porphyr. Phthalocyanines* **2000**, *4*, 727.

42. Araki, K.; Toma, H. E.; *J. Coord. Chem.* **1993**, *30*, 9.

43. Vogel, G.C.; Beckmann, B. A.; *Inorg. Chem.* **1976**, *15*, 483.

44. Bhyrappa, P.; Krishnan, V.; Nethaji, M.; *J. Chem. Soc. Dalton Trans.* **1993**, *12*, 1901.

45. Araki, K.; Toma, H. E.; *J. Photochem. Photobiol. A-Chem.* **1994**, *83*, 245.

46. Araki, K.; Toma, H. E.; *J. Chem. Res. S* **1994**, *7*, 290.